Solution Study of Engineered Quartz Binding Peptides Using Replica Exchange Molecular Dynamics

Rebecca Notman,*,† E. Emre Oren,‡ Candan Tamerler,‡ Mehmet Sarikaya,‡ Ram Samudrala,§ and Tiffany R. Walsh†,||

Department of Chemistry and Centre for Scientific Computing, University of Warwick, Coventry, CV4 7AL, United Kingdom, Genetically Engineered Materials Science and Engineering Center, and Departments of Materials Science and Engineering and Microbiology, University of Washington, Seattle, Washington, United States

Received June 11, 2010; Revised Manuscript Received October 1, 2010

We use replica-exchange molecular dynamics (REMD) to interrogate molecular structures and properties of four engineered dodecapeptides (in solution, in the absence of a surface) that have been shown to bind to quartz with different propensities. We find that all of the strong-binding peptides feature some polyproline type II secondary structure, have less conformational freedom, and feature fewer intrapeptide hydrogen bonds compared with the weak binder. The regions of contiguous proline content in a given sequence appear to play a role in fostering some of these properties of the strong binders. For preliminary insights into quartz binding, we perform lattice-matching studies between a grid corresponding with the quartz (100) surface and the strong-binding peptide REMD structures. Our findings indicate a commonality among the putative contact residues, even for peptide structures with very different backbone conformations. Furthermore, interpeptide interactions in solution are studied. Our preliminary findings indicate that the strong-binder interpeptide contacts are dominated by weak, nonspecific hydrophobic interactions, while the weak-binding peptide shows more variable behavior due to the distribution of charged residues. In summary, the solution structures of peptides appear to be significant. We propose that these differences in their intra- and interpeptide interactions can influence their propensity to bind onto a solid substrate.

Introduction

Proteins and peptides play a vital part in biology due to their incredible range of catalytic, structural, and regulatory functions. One important role of these macromolecules is to control the formation of biological hard tissues such as dental tissues, bones, and mollusc shells.[1−7] In materials science, there has been a recent surge of research toward exploiting this implicit functionality of proteins and peptides to synthesize and assemble inorganic nanomaterials under ambient conditions.[6] A significant advancement toward this goal is the identification of peptides that can bind to specific solid engineered materials and minerals.[6,8−12] The molecular mechanisms underlying the peptide−inorganic interactions, however, still remain poorly understood. Such an understanding is essential if progress is to be made in the rational design of peptides that have specific binding, synthesis, and assembly properties for use in the formation of materials in technological and medical applications.[13−15]

In recent years, numerous studies have been reported that identify peptide sequences that bind to, for example, metals, semiconductors, oxides, and carbon materials.[8,6,16,17,9,18−21] The interactions of peptides with silica surfaces are of significant interest due to the prevalence of silica in nature and its applications in engineering and biomaterials. For example, naturally occurring silica-biocomposites are found in the skeletons or cell walls of several marine organisms such as diatoms and sponges[22] and there is much interest in the proteins/peptides (and their mimics) that direct silica synthesis.[23−28] The synthesis of silica nanostructures is also important due to their potential applications in catalysis, nanophotonics, and electronics.[29]

The broad topic of the adsorption of amino acids onto inorganic solid surfaces has been the subject of a recent review.[30] In particular, there have been a number of experiments to investigate the adsorption of organic and biomolecules onto silica surfaces, for example, see ref 31 and references therein. Churchill et al.[31] measured the adsorption of six amino acids onto quartz surfaces at different pH and found that the greater the charge difference between the amino acid and the surface, the stronger the adsorption, due to the electrostatic interaction. This is in agreement with Vlasova and Golovkova[32] who studied the interaction of a series of amino acids with amorphous silica and found that, at a given pH, only the amino acids carrying a net positive charge were adsorbed onto the surface. In a study of the adsorption of serine and leucine onto hydrophilic and hydrophobic quartz surfaces, leucine was shown to have a higher free energy of adsorption onto both surfaces than serine did.[33] Very recently, solid-state nuclear magnetic resonance spectroscopy has been used to investigate the adsorption of glycine onto silica surfaces.[34] In addition, a number of theoretical studies focused on characterizing the adsorption of amino acids onto quartz and silica, using both using electronic structure theory and molecular simulation have recently appeared.[35−38] The interfacial environment modeled in these studies ranges from the gas phase through to fully solvated with water. However, while studies of single amino acid adsorption are valuable, it

* To whom correspondence should be addressed. E-mail: r.notman@warwick.ac.uk.
† Department of Chemistry, University of Warwick.
‡ Department of Materials Science and Engineering, University of Washington.
§ Department of Microbiology, University of Washington.
|| Centre for Scientific Computing, University of Warwick.

10.1021/bm100646z
Published on Web 10/22/2010

Table 1. Sequences of the Three Strong Binding Peptides S1, S2, and S3 and the Weak Binding Peptide W1

peptide	sequence
S1	PPPWLPYMPPWS
S2	LPDWWPPPQLYH
S3	SPPRLLPWLRMP
W1	EVRKEVVAVARN

must be noted that the effects of these residues within a protein or peptide are not simply additive, and the binding behavior cannot be predicted from knowledge of the amino acid composition alone. Furthermore, the carboxylate and ammonium termini of the amino acids, which may interact with the surface (as seen in many of the theoretical studies mentioned above), are blocked when the amino acids are linked together in a peptide.

Recent studies of peptide adsorption onto silica surfaces include the adsorption of a 14-amino acid amphiphilic peptide onto hydrophilic silica[39,40] and the induction of a well-defined structure in a peptide upon adsorption onto silica nanoparticles.[41] In these studies, the presence of basic side-chains was considered to be important for adsorption. In terms of proteins, the adsorption of immunoglobulin G[42] and bovine serum albumin (BSA)[42−44] on different silica surfaces has been investigated by infrared spectroscopy and circular dichroism (CD) spectroscopy. These data suggested that the carbonyl groups of BSA interacted with vicinal hydroxyl groups, while the imido groups interacted with isolated hydroxyl groups of the silica surface. In terms of probing the links between peptide conformation and silica binding affinity, Seker et al.[45] experimentally characterized the surface binding of combinatorially selected silica binding peptides using surface plasmon resonance spectroscopy (SPR), reporting the free energy of adsorption. More importantly, this worked tested multiple repeats of the peptide sequences to investigate if an increase in the binding affinity scaled with an increase in the number of binding domains. No general trend was found in binding strength upon increasing the number of repeat units from one to three, suggesting that conformational changes between the single- and multiple-repeat peptides played a significant role in the modes of surface binding.

Recently, Oren et al. reported a bioinformatics approach that was used to design peptide sequences with a predictable binding affinity for silica, informed by the results of combinatorial selection and characterization of quartz-binding peptides.[46] A set of these predicted strong and weak binders were chosen to be synthesized and the binding was quantitatively characterized using SPR spectroscopy, with the designed peptides exhibiting affinities to quartz as predicted.[46] The sequences of three of the strong-binding designed quartz binders, referred to as S1, S2, and S3, and one of the designed weak-binding quartz binders, referred to as W1, are given in Table 1. Interestingly, the strong-binding peptides contain predominantly nonpolar, neutral amino acids, which suggests that electrostatic interactions might not provide the main driving force for binding. In our previous simulation studies of water and amino acid analogues binding to quartz surfaces, we found that the free energy to adsorb nonpolar moieties onto the quartz (100) surface is favorable.[47] Small hydrophobic groups are able to sit in hydrophobic interstices on the surface, where they are shielded from the solvent. Because the content of S1, S2, and S3 comprises mostly nonpolar residues, this type of interaction may be important for the binding of these peptides to quartz.

Previous studies have suggested that both the amino acid composition and the amino acid sequence are important for binding.[18,45,46] Together these properties govern the three-dimensional structures of the peptides, which in turn must determine the availability of certain residues presented to the surface, and thus, at least to first order, any spatial or lattice matching of residues with surface sites. Analysis of the content of the strong quartz binders compared to the weak binders has indicated[46] that the strong binding peptides may adopt extended conformations due to the conserved occurrence of residues with bulky side chains (e.g., Trp, Phe, Met) and the presence of proline, which is known to reduce conformational flexibility. In addition, CD spectral analysis of the designed peptides shows that the strong binders adopt a polyproline II (PPII) secondary structure, whereas the weak binders are classified as random coil.[48] While these observations provide clues to the possible mechanisms of binding, it is clear that in order to ascertain the relationship between the peptide sequences and their quartz-binding function, it is necessary to investigate the structural and conformational properties of these sequences in more detail.

In recent years computer simulation has become a powerful tool for the study of molecular systems in atomistic detail. There have been numerous computational studies of amino acids, peptides, and proteins in both the gas and the solution phases using ab initio and molecular dynamics (MD) techniques.[49] Methods such as simulated tempering[50] or replica exchange molecular dynamics (REMD)[51] have become popular ways to improve the sampling of the peptide configurational space and avoid trapping the peptide in a local minimum on the potential energy surface. For example, REMD has recently been successfully applied to a fragment of the prion protein to make structural predictions that were confirmed with CD spectroscopy.[52] In terms of peptides selected for binding to surfaces, a similar approach, namely, simulated tempering Monte Carlo simulations, has been previously reported in the study of the solution behavior of GaAs- and Si-binding peptides.[53] Approaches to improve the efficiency of REMD as applied to peptides in solution is an active area of research.[54] Application of these approaches to the study of the properties of quartz binding peptides will provide valuable insights into the molecular mechanisms that facilitate peptide recognition of and binding to solid materials. In particular, it is desirable to understand how the primary residue sequence and secondary structure play a role in the recognition and binding of these peptides to quartz.

Recently,[48] we carried out some initial simulations of the two strong quartz-binding peptides, and one weak quartz-binding peptide, in the presence and absence of the quartz (100) surface. In this paper we extend this work and present REMD simulations (in solution only, without any surface present) of three designed peptides with strong quartz-binding affinity and one designed peptide with weak affinity, including one peptide not previously studied by molecular simulation. We aim to explore the characteristics of the peptides in solution (both as isolated single chains and as pairs of peptides), to gain insights into the possible mechanisms by which these peptides bind to quartz surfaces. We have included a comprehensive analysis of the structure and properties of the peptides and also consider the role of peptide dimerization. Furthermore, we have used the results of our REMD simulations to inform lattice matching calculations. The lattice matching approach is used to identify putative binding configurations of the peptides on the quartz (100) surface.

Simulation Methodology. *Details of the Simulations.* For the simulations of the peptides in water, we used REMD[51] as implemented in the Gromacs package, version 3.3.3.[55] REMD

is a method to enhance the sampling of phase space in an MD simulation. It is based on the idea that simulations run at high temperatures can be used to overcome energetic barriers and obviates some of the sampling problems associated with the presence of multiple-minima. In practice, several noninteracting replicas of the system are run at different temperatures. After a specified number of time steps, exchanges are attempted between simulations at neighboring temperatures. As shown in ref 57 in the NPT ensemble, the acceptance probability of making an exchange between replicas i and j is given by

$$P(i \leftrightarrow j) = \min\left(1, \exp\left\{-\left[\left(\frac{1}{k_B T_i} - \frac{1}{k_B T_j}\right)(U_j - U_i) + \left(\frac{P_i}{k_B T_i} - \frac{P_j}{k_B T_j}\right)(V_j - V_i)\right]\right\}\right) \quad (1)$$

where T_i and T_j are the reference temperatures, U_i and U_j are the instantaneous potential energies, P_i and P_j are the reference pressures, and V_i and V_j are the instantaneous volumes of replicas i and j, respectively.[56] We simulated 22 replicas of the system at the following temperatures (in K): 294.48, 299.01, 303.59, 308.15, 312.81, 317.55, 322.32, 327.14, 332.01, 336.92, 341.90, 346.92, 352.01, 357.14, 362.36, 367.49, 372.79, 378.16, 383.57, 389.05, 394.58, 400.19. The temperatures were generated using an online temperature generator for REMD simulations.[57] To generate the starting configurations for each replica, we performed a 4 ns simulation at 400 K and then randomly selected 22 configurations from this trajectory. Each replica was then equilibrated for 1 ns at the appropriate temperature and used as a starting point for the REMD. The REMD simulations were 10 ns in duration, yielding a 220 ns total simulation time for each peptide. Exchanges between replicas were attempted every 1 ps and the exchange probability was approximately 0.1 between each replica.

The peptides were modeled using the CHARMM[58,59] forcefield and water was modeled using the modified TIP3P potential.[60,61] Each peptide was solvated in a cubic box of 4063 water molecules. Chloride counterions were included in the simulations of S3 and W1 to achieve charge neutrality. A time step of 1 fs was used throughout. A dual-range cutoff method was used for the Lennard−Jones interaction, with the radii set to 1.0 and 1.2 nm, and the neighbor list updated every 10 steps. The electrostatics were treated using particle mesh Ewald, with a real-space cutoff of 1.2 nm. Full periodic boundary conditions were employed in all directions. The simulations were carried out in the NPT (isothermal−isobaric) ensemble; the temperature of the system was controlled by the Nosé−Hoover thermostat,[62,63] and the pressure was coupled isotropically to 1 bar using the Parrinello−Rahman scheme.[64,65] Coordinates were saved every 1 ps.

To gain insights into the interactions between peptides, we also performed a total of four additional simulations of 10 ns each for either a pair of S1 molecules or a pair of W1 molecules in water (two starting configurations per pair). The temperature was set to 303.59 K. All other forcefield and simulation parameters were as described above. Replica exchange was not used for these simulations. The interaction energies between each peptide dimer were evaluated by summing the interpeptide nonbonded terms (the Lennard−Jones interaction and the short and long-ranged parts of the electrostatic interaction). A full description is given in the Supporting Information, including a complete account of how the long-ranged electrostatic component was obtained.

Details of the Clustering Analysis. A clustering algorithm[66] was used to identify related conformations of the peptides from the trajectory. To find clusters, the root-mean-squared deviation (rmsd) of the backbone atom positions between all pairs of structures was determined. For each structure, the number of neighbors for which the rmsd was 0.2 nm or less was counted. The structure with the largest number of neighbors was selected and eliminated, along with its neighbors, from the pool of structures. This procedure was repeated for the remaining structures in the pool until all structures had been assigned to exactly one cluster.

Analysis of Chain Flexibility. To further quantify and explore chain flexibility, we calculated a chain-position-dependent "localized stiffness" length scale associated with each residue in each peptide chain. Essentially, for every frame of each of the four REMD trajectories, we picked each residue and calculated the persistence of the backbone configuration both forward and backward from that point in the chain, in terms of repeat unit lengths of the peptide. Specifically, we constructed a vector, v_i, associated with the i^{th} α-carbon in the chain, defined by the left-hand adjacent backbone nitrogen and the right-hand adjacent carbonyl carbon. For each residue, we calculated the dot product, $d_i = \mathbf{v}_i \cdot \mathbf{v}_{i+1}$, such that 11 dot products were calculated per frame. We then calculated the average of each d_i, denoted $\bar{d}_i$, over all frames in the trajectory. We then picked the i^{th} residue, and for each frame, calculated the absolute deviation of d_i with respect to $\bar{d}_i$ and then counted forward along the chain from the i^{th} point (increasing in i) the integer number of repeat units, u_{if} (where the subscript f denotes "forward"), for which this absolute deviation remains below an arbitrary cutoff value (chosen here to be 0.1). We then calculated an average of u_{if} over all frames, giving $\bar{u}_{if}$ for each residue in the chain. Similarly, we also performed this counting and averaging procedure in the reverse direction (decreasing in i), to yield u_{ir} and $\bar{u}_{ir}$. We summed the $\bar{u}_{if}$ and $\bar{u}_{ir}$ to give $\bar{u}_i$, which defines a chain-position-dependent length scale of backbone stiffness, both forward and backward along the chain, at each position in the chain. A larger value of $\bar{u}_i$ indicates a longer region around that particular residue where the backbone conformation is persistent, while a value of less than 1 reveals no persistence on average for that particular residue.

Lattice Matching Protocol. Putative binding configurations of the peptide on the quartz (100) surface were identified using a lattice matching approach inspired by the work of Dai and Evans.[67] A two-dimensional grid of points was constructed, where the coordinates of the grid corresponded to the positions of the topmost layer of Si atoms on a hydroxylated quartz (100) surface and also to the positions of the hydrophobic interstices on the surface. The distances between the Si-site grid points was 0.62 nm along the [0001] direction and 0.55 nm along the [0100] direction, corresponding with the equilibrated quartz (100) surface from a previous study.[47] The hydrophobic interstitial sites were taken to be the midpoint between four Si-site points. Our previous simulations have identified these hydrophilic and hydrophobic lattice points as possible interaction sites for amino acid residues with quartz surfaces.[47] To identify peptide conformations where the atomic positions of the peptides match these lattice points, we developed a procedure to score each configuration with respect to the number of lattice matches. Each peptide was initially positioned so that its minimum height (i.e., the perpendicular distance of the closest peptide atom to the lattice) was 0.1 nm. We then score each configuration based on the following protocol. The lateral distance, d_{xy}, of each peptide atom to its nearest lattice point is calculated. If $d_{xy} <$

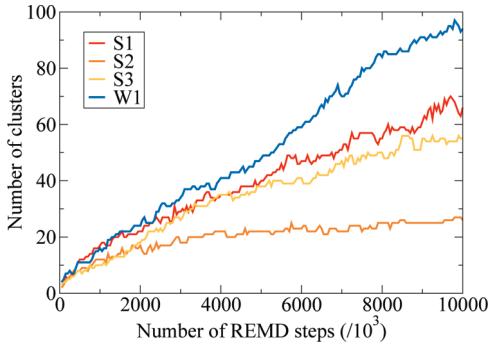

Figure 1. Number of clusters as a function of REMD steps for the strong (S1−S3) and weak (W1) binding peptides.

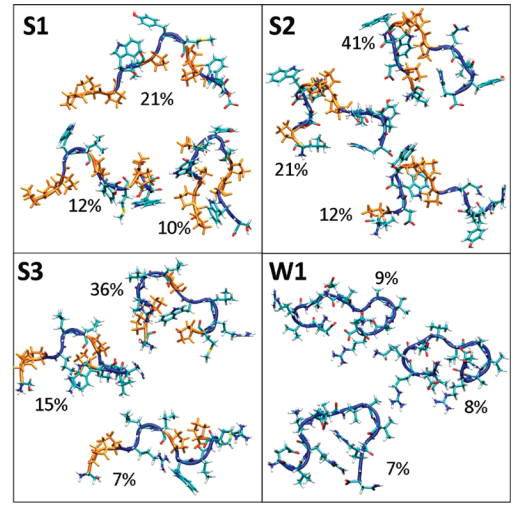

Figure 2. Central structures of the top three clusters of each peptide, with proline residues highlighted in orange. Also indicated are the percentage of the total population of structures that each cluster contains.

0.14 nm, that is, the atom is local to the lattice point, the perpendicular distance, d_z, of the atom to the surface is determined. A score of one is given for every atom within $d_z =$ 0.4 nm and a score of two is given for every atom within $d_z =$ 0.2 nm. These distances correspond to minima in the free energy profile for amino acid analogues as they approach the quartz (100) surface.[47] The lateral distance d_{xy} is then subtracted from the score, which introduces an additional penalty for displacement from the lattice site and helps to distinguish between configurations that would otherwise have the same score. The scores for each atom are summed over the entire peptide to give a total score for each peptide configuration. Note that this was simply a spatial matching procedure and does not include an energetic calculation, nor does this account for deformation of the peptide upon adsorption or the influence of the structure of the solvent at the interface. These results therefore represent a first-step toward identifying putative contact points for exploration in future work. The search was carried out over translations in x and y (the surface plane) and complete rotations about x, y, and z, with the height being renormalized to 0.1 nm after every rotation. For each peptide configuration, 61731 rotations or translations were considered and the highest scoring configurations were output for analysis. This procedure was carried out for the central structures of the top four clusters of each strong binding peptide. As the clustering analysis only considered the rmsd of the backbone structure, the positions of the side chains in the central structure are not necessarily fully representative of the structure of the peptide. Therefore, we generated additional starting structures for the lattice matching by carrying out 200 ps long simulations of each of the central structures in solution, where the positions of the backbone atoms were fixed, but the side-chain atoms were free to move. From these trajectories, an additional three configurations were selected for the lattice matching. Thus, for each peptide, 16 configurations were used in the lattice matching (the four central structures, each with four different side-chain configurations). A similar, but not identical, approach was recently described by So et al.[68] in identifying what these authors termed a "docking surface" between a gold-binding peptide and the underlying lattice of the Au(111) surface.

Results

Single-Chain Peptide-in-Solution Studies. *Structure and Conformation of the Peptides.* A clustering algorithm was used to select peptide conformations with the same (within a tolerance) backbone structure from the trajectory. The number of clusters as a function of REMD steps is presented in Figure 1. By way of comparison, a 10 ns trajectory of S1 without replica exchange yielded only 12 clusters, in contrast with the 65 clusters obtained for S1 using REMD. It appears that, in the simulations of the strong binders, the number of clusters versus time begins to converge to a constant value, but may not quite be converged yet (vide infra). We have further probed the convergence of our REMD simulations by calculating rolling averages of the relevant properties calculated herein for each peptide as a function of the number of REMD steps (vide infra); the percentage population of clusters, the average number of intrapeptide hydrogen bonds, and the localized flexibility metric. These data are summarized in Figures S2−S4 of the Supporting Information and demonstrate that, taken as a whole, the properties of interest investigated in this work are more-or-less converged with respect to the duration of the REMD runs. We note that, in individual peptide cases, there may be one piece of evidence that appears less convincing than the rest of these data, but we maintain there is sufficiently little change in most cases for each peptide, such that the broad picture of convergence emerges. This convergence analysis also applies to REMD work reported from our previous study.[48] A key finding is that we observed between 26 and 61 clusters for the strong binders, whereas we observed 94 clusters for the weak binder. This suggests that the weak binder can access a greater number of energetically favorable conformations compared with the strong-binder sequences. Traditional, global measures of chain flexibility (and/or conformational freedom) such as the average radius of gyration and end-to-end distance were calculated, but appeared invariant to the differences among the four peptides (see Figure S1, Supporting Information). Therefore, to further investigate the conformational freedom of the peptides, we instead performed a localized stiffness analysis on the peptide backbone (vide infra) that measured backbone flexibility as a function of position in the chain.

Snapshots of the central structure of the three dominant clusters of each peptide are presented in Figure 2. The snapshots suggest that the conformations of the strong binders are dominated by the presence of proline. The proline-containing regions of the strong binders appear essentially rigid, while the residues flanking these regions possess some flexibility. Thus, we suggest that proline reduces the number of degrees of freedom of the strong binders, implying a connection with the fewer number of clusters found in these cases. To examine this

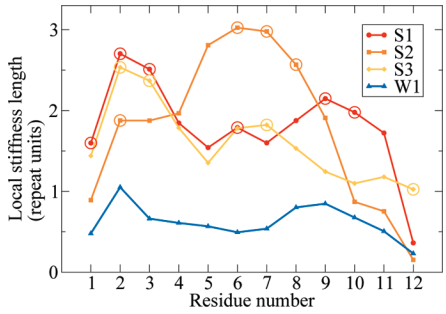

Figure 3. Local stiffness length as a function of chain position for each of the peptides. Positions that correspond with a proline residue are circled.

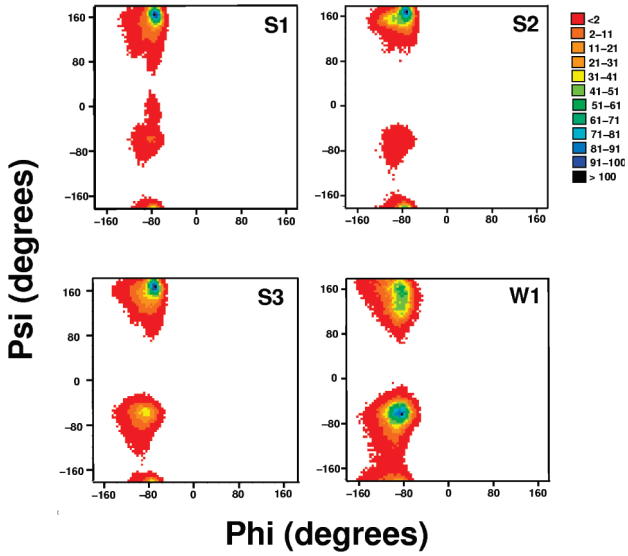

Figure 4. Ramachandran plots of each peptide, showing the distribution of the ϕ and ψ backbone angles.

further, the localized flexibility of each peptide as a function of the residue position in the sequence is presented in Figure 3. For the strong binders, it is clear that regions containing contiguous proline content introduce regions of stiffness into the chain. S1 features essentially rigid, mesogenic units at both termini and has a flexible region in the center; S2 possesses a rigid mesogenic core with flexible ends; and in general, the flexibility of S3 increases with residue number. The weak binder, which does not contain proline, is more flexible overall and lacks local regions of backbone stiffness.

Ramachandran plots for each peptide, which show the distribution of ϕ and ψ backbone angles of each residue over trajectory, are presented in Figure 4. Each of the strong binders has a distinct maximum at $\phi = -75°$ and $\psi = 160°$; a characteristic signature of PPII secondary structure. The strong-binding peptides also exhibit some random coil character. The weak binder, on the other hand, exhibits random coil conformations in equilibrium with other secondary structures such as α-helices and β-sheets. This is in good agreement with CD spectroscopic data on these systems.[48] We also searched for differences among the four peptides in terms of solvent accessible surface area. However, analysis of the hydrophilic and hydrophobic solvent accessible surface area did not produce any significant results; we simply found that the weak binder exposed more hydrophilic groups to the solvent, whereas the strong binders exposed more hydrophobic groups, which we believe is a direct result of the peptide composition.

Hydrogen Bonding. The average number of intrapeptide and peptide−water hydrogen bonds formed by each peptide is shown

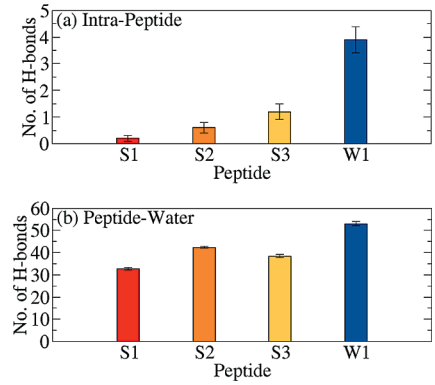

Figure 5. Average number of intrapeptide and peptide−water hydrogen bonds of each peptide.

in Figure 5. On average, the strong binders form roughly between zero and one intrapeptide hydrogen bonds, whereas the weak binder sustained an average of around four intrapeptide hydrogen bonds. The weak binder also forms more hydrogen bonds with water than the strong binders. This suggests that the weak binder is inherently more stable in water compared to the strong binders, because W1 is able to adopt conformations that maximize the number of residue−water interactions, in addition to the intrapeptide interactions. The ability of W1 to support a number of different hydrogen bonding interactions with itself and with water, in partnership with its flexibility, may help to explain the wide range of conformations that W1 can access at this temperature. The greater number of intrapeptide hydrogen bonds in W1 might act to the detriment of surface binding,[69] depending on the relative strength of the intrapeptide interactions versus the peptide−surface interactions.

Peptide Dimer Studies. Peptide association may play a part in the binding of peptides to inorganic surfaces.[68,70] For example, strong interactions between peptides may hinder binding by blocking possible residue sites for binding to the surface. Alternatively, peptide association could promote binding by a cooperative mechanism, whereby a peptide bound to the surface facilitates the attraction of additional peptides to the surface. To gain preliminary insight into the interactions between peptide chains, we performed additional simulations of pairs of S1 or W1 molecules in water. Although REMD was not used for these simulations, we can glean some valuable knowledge of the representative ways in which strong and weak binding peptides can interact with each other. We are unaware of any published atomistic simulations of interpeptide interactions for such inorganic-binding peptides. The results presented here will form a basis for a more thorough future study using more advanced sampling approaches.

Peptide−peptide interaction energies are presented in Figure 6. We point out here this interaction energy comprises a sum over nonbonded interactions between the two peptide chains over the duration of the MD trajectory, and thus does not account for energy changes associated with desolvation and solvent reorganization, nor does it account for the peptide deformation energy upon the peptides moving from free chains to the dimer complex. The interaction energy between the two S1 peptides converges to a similar value in both simulations. We observe close contacts between nonpolar residues of each peptide, but the interactions appear to be nonspecific and are probably due to a hydrophobic effect. The interaction energy of the W1 peptides fluctuates considerably during both simulations. Visual inspection of the trajectory of run 1 shows that between 0 and 4 ns the peptides are not in contact with each

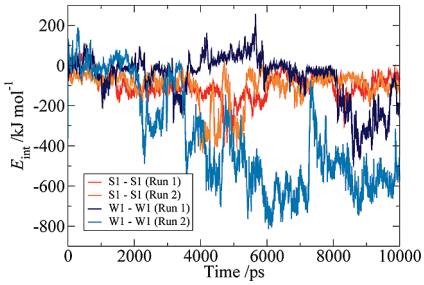

Figure 6. Interpeptide interaction energies for each simulation of pairs of S1 and W1.

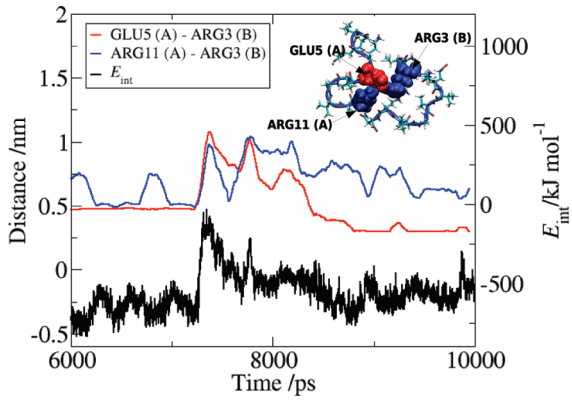

Figure 7. Distance between charge group centers as a function of time for run 2 of the pair of W1 molecules. The peptide−peptide interaction energy E_{int} is also shown for comparison. The snapshot shows the configuration of the peptides after 10 ns, where the Arg residues are shown in blue spacefill and the Glu residue in red spacefill, and the residues are labeled A and B to distinguish between the two peptide molecules.

other. Between 5 and 6 ns, random fluctuations bring a positively charged Arg residue from each peptide into close proximity, with a concomitant increase in the interaction energy. At approximately 7 ns, hydrophobic contacts are made between the Ala and Val residues of both peptides, which results in a decrease in the interaction energy. The resulting metastable dimer has the hydrophobic groups of each peptide interacting with each other, with the charged residues protruding into the solvent. We suggest that this hydrophobic association of the peptides occurs at the expense of intrapeptide hydrogen bonding (vide infra). The trajectory of run 2 from 6 to 10 ns reveals that W1 can also form a more stable complex where the negatively charged Glu5 residue of one W1 molecule pairs up with the positively charged Arg 3 residue of the other W1 molecule. The Glu5 also participates in an interpeptide interaction with Arg11. However, this arrangement brings the Arg11 into close proximity with the Arg 3 on the other W1 chain. As seen for run 1, there is an associated energetic penalty for the close contact between these two Arg residues. Figure 7 shows that the centers of the charge groups in these residues are in close proximity in this bound configuration, and that the trend in the interaction energy closely follows the residue−residue distances. The snapshot of the system at 10 ns in Figure 7 illustrates the W1 peptides binding to each other via this electrostatically-driven mechanism.

The average number of intrapeptide and interpeptide hydrogen bonds in each of the dimer systems is given in Table 2. On average, S1 forms less than one interpeptide hydrogen bond, which supports our suggestion that there are no specific interactions between S1 molecules. For W1, we examined the average number of intrapeptide and interpeptide hydrogen bonds

Table 2. Number of Intrapeptide Hydrogen Bonds for the First (AA) and Second Peptide (BB) and Interpeptide Hydrogen Bonds (AB)[a]

peptide	AA	AB	BB
S1 (run 1)	0.3	0.5	0.2
S1 (run 2)	2.0	0.8	0.1
W1[b]	4.0	0.0	6.0
W1[c]	2.0	1.0	5.0
W1[d]	6.0	4.0	3.0

[a] For S1, the averaging is over the entire simulation. For W1, the trajectory is first divided into unbound and bound configurations. [b] Unbound. [c] Hydrophobic binding. [d] Electrostatic binding.

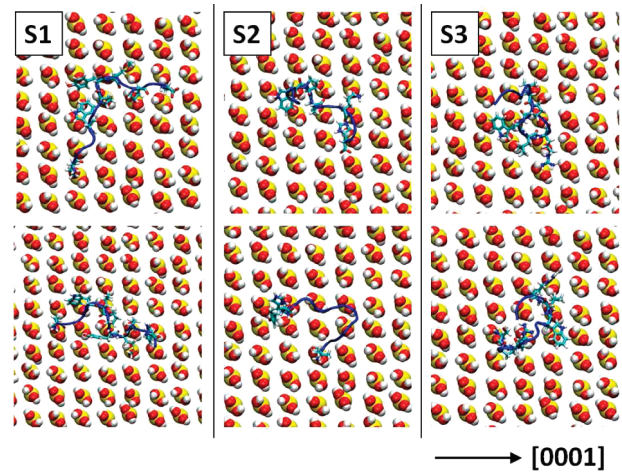

Figure 8. Highest scoring configurations and orientations of each of the strong binders, identified from the lattice matching procedure, shown as plan views.

for the unbound dimer configurations, the dimer configurations where the peptides are bound via the hydrophobic residues and the dimer configurations where the peptides are bound via charge−charge interactions. As shown in Table 2, the unbound peptides form 4−6 intrapeptide hydrogen bonds, which is in alignment with our results for a single peptide in solution. The W1 dimer bound via hydrophobic interactions has fewer hydrogen bonds overall, as there is a tendency for the polar residues to point out toward the solvent in this configuration. For the dimer where the W1 molecules interact via the charged residues, four interpeptide hydrogen bonds are formed, with this occurring at the expense of only one intrapeptide hydrogen bond overall. Therefore, as well as the electrostatic interactions, hydrogen bond formation may also be responsible for the increase in the binding strength as these peptides associate. Overall, the results suggest that S1 weakly associates in a nonspecific manner, whereas the behavior of W1 seems more variable due to the presence of several charged residues, where a mixture of positive and negative charge is present.

Lattice Matching Studies. The two highest scoring configurations of each peptide identified by the lattice matching study are presented in Figure 8. Other than the peptide backbone, only the residues that have any of their atoms within 0.4 nm of the surface are shown. These residues are thus identified as putative contact residues and are listed in Table 3, where we also give the cluster number of the peptide structure. The distribution of scores with test configuration number (rotation or translation), is shown for the top-scoring cluster of each peptide in Figure S5 in the Supporting Information. These data indicate that the top-scoring arrangements of each peptide are distinct from the bulk of the arrangements explored overall. We point out here that, given the simplicity of our lattice-matching approach, it is

Table 3. Cluster Number and Matched Residues (Underlined and in Bold Face) for the Top Two Scores for Each of the Strong Binders, Obtained from the Lattice Matching Studies

peptide	cluster	residues within 0.4 nm
S1	01	**P**PP**W**L**PYM**P**P**W**S**
S1	02	**P**PP**WLPYMP**P**W**S
S2	03	LPDW**WPP**P**Q**LY**H**
S2	01	**L**PDWWPPPQL**YH**
S3	01	SPPRL**LPWLR**MP
S3	03	**SP**P**R**LLP**WLR**MP

not appropriate to compare scores between different peptides; rather, it is intended for comparison between different arrangements of the same peptide. A higher score for one peptide compared with another does not necessarily indicate that this peptide is predicted to bind more strongly to the surface.

It is interesting to note that even though the backbone configurations of the top two matched structures are different, we observe commonality among the types of residues that form the putative contact points. A current hypothesis in bio-inorganic recognition is that strong binding sequences can bind in many different ways to the surface,[69,71−73] and our observations are consistent with this. For S1, the highest-scoring arrangement was oriented with five nonpolar neutral residues close to the surface (Pro1, Trp4, Pro6, Met8, and Pro10). It is feasible that, if this structure was used in MD simulations, these residues might be attracted to the hydrophobic interstices on the quartz surface as previously observed in our simulations of an alanine analogue on quartz.[47] In this arrangement, Trp4 is oriented flat on the surface where it would also be able to participate in π-hydrogen bonds with the hydroxylated surface. The other matched residues were Tyr7 and Ser12. Both of these residues contain a hydroxyl group and would therefore be expected to form hydrogen bonds with the surface silanol groups, if deployed in MD simulations. The second highest scoring configuration for S1 matched eight residues which, notably, included an additional Leu and Trp residue. It would be expected that binding in this configuration would occur via a mechanism similar to that described above. The highest scoring arrangement of S2 also featured Trp and Pro as contact residues and the second highest scoring arrangement featured only three contact residues: Leu 1, Tyr 11, and His 12. In the arrangement for the latter contact residue, as shown in Figure 8, the imidazole ring may be able to participate in hydrogen bonds with the surface silanol groups. Our lattice matching study also identified Arg, Leu, Trp, and Pro as putative binding residues for S3. Leu is likely to interact via the hydrophobic mechanism described above, whereas Arg may form hydrogen bonds with the surface. Overall, these results are in good agreement with the bioinformatics studies by Oren et al.[46] where Pro, Trp, and Leu were proposed as important residues for the binding of these peptides to quartz. Our recent findings, obtained from a combination of bioinformatics and MD studies, also revealed this finding.[48] Of course, this lattice matching procedure is only a first step toward identifying the mechanisms of binding and it does not take into account the physiochemical interactions of the peptide with the surface or the structural rearrangements of the peptide that may take place upon binding. We are extending these studies to MD simulations of the peptides interacting with quartz surfaces, which in the future will address these issues in detail.

Discussion

The use of REMD in this work shows that it is possible to approach a description of equilibrium conditions for these dodecapeptides in solution, as evidenced by our convergence data (Figure 1 and Figures S2−S4, Supporting Information). We are unaware of any other published atomistic simulations on inorganic binding peptides that has attempted to quantify this convergence to such a degree before. It would appear that, from our work, at least 10 ns of REMD would be required to adequately equilibrate such dodecapeptides in solution (without the presence of the surface). This is particularly important when calculated estimates of peptide-surface binding energies are sought using the "compartmentalization" protocols of Yang et al.[74] or Heinz,[75] because these protocols require a robust evaluation of energy of the equilibrated peptide-solution system. Our findings caution that use of conventional MD in obtaining these peptide-solution energies may be inadequate.

The results of the cluster and flexibility analyses indicate that proline can reduce the conformational flexibility, in a localized sense, of the strong binders. As proline-rich content is a recurring theme among the strong quartz-binding sequences,[46] we propose that there is a link between presence of contiguous regions of proline content, conformational flexibility, and strong quartz-binding function. The rigidity that proline-rich regions can impose on a peptide backbone may prevent strong, competitive intrapeptide interactions from forming. Previous simulations of the peptide-titania interface suggest that such intrapeptide interactions may be detrimental to surface binding, in the sense that key surface-binding residues involved in intrapeptide interactions may become unavailable for surface binding.[69] Furthermore, the constraints imposed by the regions of contiguous proline may present the flanking residues in the best position for surface binding. In the present case, the lattice matching studies indicate that even though the backbone structures of the largest clusters are distinct, there is commonality among the types of residues that make contact with surface sites. It may therefore be the case that proline restricts the configurations of the strong binders to those where key residues are available for binding to the surface. An additional consideration is the potential loss in conformational entropy of the peptide upon binding, which will be less for rigid molecules than for flexible molecules.[76] It should be pointed out that several studies of peptides binding to inorganic surfaces have indicated that increased conformational flexibility (in a global sense) *improves* binding affinity.[77] The proposed explanation is that flexible molecules are able to undergo rearrangements that promote binding to the surface. Peelle et al.[19] expanded on this by showing that increased conformational flexibility (in a global sense) improved binding affinity, while the addition of residues that introduced structural constraints improved binding specificity. Clearly, there might be a compromise required for high binding affinity. We have shown that the S1−3 peptides can adopt a range of structures while also possessing rigid mesogenic segments that prevent complete conformational freedom. Our findings indicate that an analysis that weighs the balance between localized flexibility and localized stiffness may provide more insight than a property that is informed by a global flexibility metric (such as radius of gyration). In other words, it may not be sufficient to merely state that a peptide if flexible or not, in a global sense. Rather, we suggest that a more useful analysis can be provided via identification of where the peptide is flexible and where it is stiff and, furthermore, by making correlations between these flexible/stiff regions with areas of the chain that contain putative surface-binding residues.

Our analyses indicate that the strong binders form fewer intrapeptide hydrogen bonds compared with the weak binder. The strong binders largely comprise nonpolar, neutral, residues

that do not feature strong intrapeptide or interpeptide interactions. The weak binder, on the other hand, contains a number of polar and charged residues, which enables it to form stabilizing interactions within the molecule or with other W1 molecules. For example, there might be a barrier to W1 binding to the surface, associated with overcoming the intrapeptide and, possibly, interpeptide interactions. The interaction with water may also be a contributing factor; interaction of the strong binders with quartz may shield the hydrophobic residues from unfavorable interactions with the solvent.[47] On the other hand, W1 forms a greater number of hydrogen bonds with the solvent than the strong binders, which might not be sufficiently compensated for by interactions with the surface.

Conclusions

In summary, we have presented results of REMD simulations for single chains of peptides in solution, where these peptides have been shown previously to exhibit different binding properties to quartz. Our simulations make direct contact with secondary structure characterization experiments, giving validation support to the CHARMM force field while also underscoring the necessity of using advanced sampling approaches such as REMD, compared with conventional MD. The secondary-structure characteristics of the peptides themselves are distinctly different between the strong binders and the weak binder. We have linked these differences to physically transparent properties of the peptides inferred from our REMD simulations, namely, the local flexibility metric and the degree of intrapeptide interaction (indicated by the average number of intrapeptide hydrogen bonds). We proposed that the local stiffness in the strong-binding peptides confers a range of advantages with relation to favorable binding on the quartz surface: (i) the mesogenic-like segments in these peptides may facilitate favorable presentation of key hydrophobic residues to the quartz surface, (ii) this rigidity appears to arise from the presence of contiguous proline in the sequences, while proline itself is predicted to have a good affinity for quartz surfaces,[47] and (iii) these localized regions of rigidity appear to play a role in limiting the degree to which the strong-binding peptides can self-interact. Moreover, our findings have suggested that interpeptide interactions also may play a role in peptide-surface binding; our results suggest that the strong-binder interpeptide interactions are different to those seen for the weak binder. With further in-depth investigation, it may be possible to explore whether or not interpeptide interactions can actually hinder surface binding. All of our findings suggest that we can harness elements of localized stiffness and spatial positioning of residues, to minimize the occurrence of intrapeptide interactions and maximize the presentation of key binding residues. These two suggestions make a modest start on the path to rational design of peptides with controllable properties at interfaces with inorganic materials.

Acknowledgment. R.N. and T.R.W. wish to acknowledge the computer facilities of the Centre for Scientific Computing, University of Warwick, and the use of the U.K. National Grid Service in carrying out this work. The funding for this project was provided by the EPSRC (Grant EP/E02095X/1) and also by the NSF-MRSEC program via GEMSEC, a member of the Materials Facilities Network, at the University of Washington (E.E.O., C.T., R.S., and M.S.).

Supporting Information Available. Plots of radius of gyration and end-to-end distance as a function of the number of REMD steps, additional methodology explaining the calculation of dimer interaction energies, plots of percentage of cluster populations as a function of REMD steps, changes in the local flexibility metric profile as a function of REMD steps, plots of the rolling average of the number of intrapeptide hydrogen bonds as a function of REMD steps, and histogram of lattice matching scores for each peptide. This material is available free of charge via the Internet at http://pubs.acs.org.

References and Notes

(1) Mann, S. *Nature* **1988**, *332*, 119–124.
(2) Weiner, S.; Addadi, L. *J. Mater. Chem.* **1997**, *7*, 689–702.
(3) Sarikaya, M. *Proc. Natl. Acad. Sci. U.S.A.* **1999**, *96*, 14183–14185.
(4) Paine, M. L.; Krebsbach, P. H.; Chen, L. S.; Paine, C. T.; Yamada, Y.; Deutsch, D.; Snead, M. L. *J. Dent. Res.* **1998**, *77*, 496–502.
(5) Belcher, A. M.; Wu, X. H.; Christensen, R. J.; Hansma, P.; Stucky, G. D.; Morse, D. E. *Nature* **1996**, *318*, 56–58.
(6) Sarikaya, M.; Tamerler, C.; Jen, A. K. Y.; Schulten, K.; Baneyx, F. *Nat. Mater.* **2003**, *2*, 577–585.
(7) Olszta, M. J.; Cheng, X.; Jee, S. S.; Kumar, R.; Kim, Y. Y.; Kaufman, M. J.; Douglas, E. P.; Gower, L. B. *Mater. Sci. Eng., R* **2007**, *58*, 77–116.
(8) Brown, S. *Nat. Biotechnol.* **1997**, *15*, 269–272.
(9) Whaley, S. R.; English, D. S.; Hu, E. L.; Barbara, P. R.; Belcher, A. M. *Nature* **2000**, *405*, 665–668.
(10) Naik, R. R.; Brott, L. L.; Clarson, S. J.; Stone, M. O. *J. Nanosci. Nanotechnol.* **2002**, *2*, 95–100.
(11) Tamerler, C.; Kacar, T.; Sahin, D.; Fong, H.; Sarikaya, M. *Mater. Sci. Eng., C* **2007**, *27*, 558–564.
(12) Evans, J. S.; Samudrala, R.; Walsh, T. R.; Oren, E. E.; Tamerler, C. *MRS Bull.* **2008**, *33*, 514–518.
(13) Seeman, N.; Belcher, A. M. *Proc. Natl. Acad. Sci. U.S.A.* **2002**, *99*, 6451–6455.
(14) Berry, C. C.; Curtis, A. S. G. *J. Phys. D: Appl. Phys.* **2003**, *36*, R198–R206.
(15) Tamerler, C.; Sarikaya, M. *ACS Nano* **2009**, *3*, 1606–1615.
(16) Naik, R. R.; Stringer, S. J.; Agarwal, G.; Jones, S. E.; Stone, M. O. *Nat. Mater.* **2002**, *1*, 169–172.
(17) Sano, K. I.; Shiba, K. *J. Am. Chem. Soc.* **2003**, *125*, 14234–14235.
(18) Goede, K.; Busch, P.; Grundmann, M. *Nano Lett.* **2004**, *4*, 2115–2120.
(19) Peelle, B. R.; Krauland, E. M.; Wittrup, K. D.; Belcher, A. M. *Langmuir* **2005**, *21*, 6929–6933.
(20) Thai, C. K.; Dai, H.; Sastry, M. S. R.; Sarikaya, M.; Schwartz, D. T.; Baneyx, F. *Biotechnol. Bioeng.* **2004**, *87*, 129–137.
(21) Wang, S.; Humphreys, E. S.; Chung, S. Y.; Delduco, D. F.; Lustig, S. R.; Wang, H.; Parker, K. N.; Rizzo, N. W.; Subramonay, S.; Chiang, Y. M.; Jagota, A. *Nat. Mater.* **2003**, *2*, 196–200.
(22) Coombs, J.; Volcani, B. E. *Planta* **1968**, *82*, 280–292.
(23) Kröger, N.; Deutzmann, R.; Bergsdorf, C.; Sumper, M. *Proc. Natl. Acad. Sci. U.S.A.* **2000**, *97*, 14133–14138.
(24) Cha, J. N.; Shimizu, K.; Zhou, Y.; Christiansen, S. C.; Chmelka, B. F.; Stucky, G. D.; Morse, D. E. *Proc. Natl. Acad. Sci. U.S.A.* **1999**, *96*, 361–365.
(25) Patwardhan, S. V.; Clarson, S. J.; Perry, C. C. *Chem. Commun.* **2005**, 1113–1121.
(26) Groeger, C.; Lutz, K.; Brunner, E. *Cell Biochem. Biophys.* **2008**, *50*, 23–39.
(27) Zhang, Y.; Wu, H.; Li, J.; Li, L.; Jiang, Y.; Jiang, Y.; Jiang, Z. *Chem. Mater.* **2008**, *20*, 1041–1048.
(28) Kroger, N.; Sandhage, K. H. *MRS Bull.* **2010**, *35*, 122–126.
(29) Yuwono, V. M.; Hartgerink, J. D. *Langmuir* **2007**, *23*, 5033–5038.
(30) Lambert, J.-F. *Origins Life Evol. Biospheres* **2008**, *38*, 211–242.
(31) Churchill, H.; Teng, H.; Hazen, R. M. *Am. Mineral.* **2004**, *89*, 1048–1055.
(32) Vlasova, N. N.; Golovkova, L. P. *Colloid J.* **2004**, *66*, 657–662.
(33) Alaeddine, S.; Nygren, H. *Colloids Surf., B* **1996**, *6*, 71–79.
(34) Lopes, I.; Piao, L.; Stievano, L.; Lambert, J.-F. *J. Phys. Chem. C* **2009**, *113*, 18163–18172.
(35) Gambino, G. L.; Grassi, A.; Lombardo, M. G.; Marletta, G. *J. Phys. Chem. B* **2004**, *108*, 2600–2607.
(36) Nonella, M.; Seeger, S. *ChemPhysChem* **2008**, *9*, 414–421.
(37) Rimola, A.; Civalleri, B.; Ugliengo, P. *Langmuir* **2008**, *24*, 14027–14034.
(38) Rimola, A.; Sodupe, M.; Ugliengo, P. *J. Phys. Chem. C* **2009**, *113*, 5741–5750.

(39) Mermut, O.; Phillips, D. C.; York, R. L.; McCrea, K. R.; Ward, R. S.; Somorjai, G. A. *J. Am. Chem. Soc.* **2006**, *128*, 3598–3607.
(40) Phillips, D. C.; York, R. L.; Mermut, O.; McCrea, K. R.; Ward, R. S.; Somorjai, G. A. *J. Phys. Chem. C* **2007**, *111*, 255–261.
(41) Lundqvist, M.; Nygren, P.; Jonsson, B. H.; Broo, K. *Angew. Chem., Int. Ed.* **2006**, *45*, 8169–8173.
(42) Giacomelli, C. E.; Bremer, M. G. E. G.; Norde, W. *J. Colloid Interface Sci.* **1999**, *220*, 13–23.
(43) Giacomelli, C. E.; Norde, W. *J. Colloid Interface Sci.* **2001**, *233*, 234–240.
(44) Tarasevich, Y. I.; Monakhova, L. I. *Colloid J.* **2002**, *64*, 482–487.
(45) Seker, U. O. S.; Wilson, B.; Sahin, D.; Tamerler, C.; Sarikaya, M. *Biomacromolecules* **2009**, *10*, 250–257.
(46) Oren, E. E.; Tamerler, C.; Sahin, D.; Hnilova, M.; Seker, U. O. S.; Sarikaya, M.; Samudrala, R. *Bioinformatics* **2007**, *23*, 2816–2822.
(47) Notman, R.; Walsh, T. R. *Langmuir* **2009**, *25*, 1638–1644.
(48) Oren, E. E.; Notman, R.; Kim, I. W.; Evans, J. S.; Walsh, T. R.; Samudrala, R.; Tamerler, C.; Sarikaya, M. *Langmuir* **2010**, *26*, 11003–11009.
(49) Daura, X. *Theor. Chim. Acta* **2006**, *116*, 297–306.
(50) Marinari, E.; Parisi, G. *Europhys. Lett.* **1992**, *19*, 451–458.
(51) Sugita, Y.; Okamoto, Y. *Chem. Phys. Lett.* **1999**, *314*, 141–151.
(52) Grabenauer, M.; Wu, C.; Soto, P.; Shea, J. E.; Bowers, M. T. *J. Am. Chem. Soc.* **2010**, *132*, 532–539.
(53) Mitternacht, S.; Schnabel, S.; Bachmann, M.; Janke, W.; Irback, A. *J. Phys. Chem. B* **2007**, *111*, 4355–4360.
(54) Li, X. F.; Latour, R. A.; Stuart, S. J. *J. Chem. Phys.* **2009**, *130*, 174106−1174106−9.
(55) Lindahl, E.; Hess, B.; van der Spoel, D. *J. Mol. Model.* **2001**, *7*, 306–317.
(56) Okabe, T.; Kawata, M.; Okamoto, Y.; Mikami, M. *Chem. Phys. Lett.* **2001**, *335*, 435–439.
(57) Patriksson, A.; van der Spoel, D. *Phys. Chem. Chem. Phys.* **2008**, *10*, 2073–2077.
(58) Brooks, B. R.; Bruccoleri, R. E.; Olafson, B. D.; Sates, D. J.; Swarninathan, S.; Karplus, M. *J. Comput. Chem.* **1983**, *4*, 187–217.
(59) MacKerell, A. D.; Brooks, B.; Brooks, C. L.; Milsson, L.; Roux, B.; Won, Y.; Karplus, M. *Encyclopedia of Compuational Chemistry*; John Wiley & Sons: Chichester, 1998; Vol. 1, pp 271−277.
(60) Jorgensen, W. L.; Chandrasekhar, J.; Madura, J. D.; Impey, R. W.; Klein, M. L. *J. Chem. Phys.* **1983**, *79*, 926–935.
(61) Neria, E.; Fischer, S.; Karplus, M. *J. Chem. Phys.* **1996**, *105*, 1902–1921.
(62) Nosé, S. *Mol. Phys.* **1984**, *52*, 255–268.
(63) Hoover, W. G. *Phys. Rev. A* **1985**, *31*, 1695–1697.
(64) Parrinello, M.; Rahman, A. *J. Appl. Phys.* **1981**, *52*, 7182–7190.
(65) Nosé, S.; Klein, M. L. *Mol. Phys.* **1983**, *50*, 1055–1076.
(66) Daura, X.; Gademann, K.; Jaun, B.; Seebach, D.; van Gunsteren, W. F.; Mark, A. E. *Angew. Chem., Int. Ed.* **1999**, *38*, 236–240.
(67) Dai, Y.; Evans, J. S. *J. Chem. Phys.* **2000**, *112*, 5144–5157.
(68) So, C. R.; Kulp, J. L.; Oren, E. E.; Zareie, H.; Tamerler, C.; Evans, J. S.; Sarikaya, M. *ACS Nano* **2009**, *3*, 1525–1531.
(69) Skelton, A. A.; Liang, T. N.; Walsh, T. R. *ACS Appl. Mater. Interfaces* **2009**, *1*, 1482–1491.
(70) Goede, K.; Grundmann, M.; Holland-Nell, K.; Beck-Sickinger, A. G. *Langmuir* **2006**, *22*, 8104–8108.
(71) Tomasio, S. D.; Walsh, T. R. *Mol. Phys.* **2007**, *105*, 221–229.
(72) Tomasio, S. M.; Walsh, T. R. *J. Phys. Chem. C* **2009**, *113*, 8778–8785.
(73) Walsh, T. R.; Tomasio, S. M. *Mol. BioSyst.* **2010**, *6*, 1707–1718.
(74) Yang, M.; Stipp, S. L. S.; Harding, J. H. *Cryst. Growth Des.* **2008**, *8*, 4066–4074.
(75) Heinz, H. *J. Comput. Chem.* **2010**, *31*, 1564–1568.
(76) Bohm, H. J.; Klebe, G. *Angew. Chem., Int. Ed.* **1996**, *35*, 2589–2614.
(77) Kantarci, N.; Tamerler, C.; Sarikaya, M.; Haliloglu, T.; Doruker, P. *Planta* **2005**, *46*, 4307–4313.

BM100646Z